Sensors & Actuators: B. Chemical 324 (2020) 128763

Contents lists available at ScienceDirect

Sensors and Actuators: B. Chemical

journal homepage: www.elsevier.com/locate/snb

An asymmetric electrode for directional droplet motion on digital microfluidic platforms

Wei Wang [1], Xichuan Rui [1], Wenjie Sheng, Qing Wang, Qi Wang, Kaidi Zhang, Antoine Riaud *, Jia Zhou *

State Key Laboratory of ASIC and System, School of Microelectronics, Fudan University, Shanghai 200433, China

ARTICLE INFO

Keywords:
Electrowetting-on-dielectric
Asymmetric design
Alternate interconnection
Directional movement
Pin-count minimization

ABSTRACT

The development of large-scale electrowetting-on-dielectric (EWOD) platforms with numerous integrated functions requires a large number of electrodes. While this challenge has traditionally been addressed by pin-count minimization strategies and circuit-routing schemes, we propose heart-shape electrodes that allow using even fewer pins when the droplet motion is unidirectional. This electrode geometry ensures that the droplet overlaps more with the front electrode than with the rear one, resulting in a net capillary force that pulls the droplet forward. Droplets with a footprint diameter between 0.8 and 1 times the electrode width can be driven reliably over long distances using only two alternately applied actuation signals. The maximum signal switching frequency that enables the reliable movement of droplets is proportional to the square of the applied voltage and the gap height, but inversely proportional to the electrode diameter. Each segment of the interconnection circuit spans only two electrode-lengths, which simplifies the circuit routing and avoids the possible trace overlap in large-scale electrode arrays. By minimizing the pin number, this asymmetric design provides a promising strategy for electrode arrangement in multifunctional, large-scale EWOD platforms.

1. Introduction

As a promising strategy for liquid handling in microfluidic systems, electrowetting-on-dielectric (EWOD) has gained increasing attention in recent years [1–7]. The integration of multifunctional components in lab-on-a-chip (LOC) applications has stimulated the development of large-scale EWOD platforms involving a large number of electrodes [8–11]. To control the growing number of EWOD electrodes, the electrode arrays must be capable of electrically addressing each electrode independently, which is commonly achieved with a multilayer arrangement of electrical connections through a multi-level metallization [11–13]. However, (i) a large number of control pins easily exhaust signal pins or ports on common microcontroller units, (ii) the multilayer electrical connections to external devices (e.g. off-chip signal generators and controllers) greatly increase structural complexity and manufacturing cost, and (iii) the high actuation voltage required for such devices is also more likely to cause crosstalk, trapped charge, and breakdown of the dielectric layer [11,13–15]. Therefore, pin-count proliferation has become a major concern for large-scale EWOD designs.

To solve this problem, a widely used approach is to assign one control pin to multiple electrodes without affecting the assay execution. In a cross-reference strategy, a set of electrodes in one row/column is connected to a single control pin [12,16,17]. This reduces the pin number (i.e. the number of actuation signals) of the N-column, M-row two-dimensional electrode array from $N \times M$ to $N + M$. However, due to the electrode crosstalk, the cross-reference scheme does not allow controlled movements of more than two droplets simultaneously. In this respect, the broadcast electrode-scheduling method [18] and network-flow-based pin-count algorithm [19] were proposed by identifying the mutually compatible actuation sequences. Pin-count-based design [20], scalable pin-constrained wiring schemes [21], and scalable heuristics [22] have been proposed to balance the layer count of electrical connections, pin count, and cost in broadcast addressing framework. Furthermore, to cope with the rapid growth of the scale, active-matrix addressing strategy with thin film transistor arrays presents another method for reconfigurable paths and high parallelizability [10]. However, these hardware solutions exponentially increase the design difficulty and droplet (circuit) routing complexity. Their

* Corresponding authors.
E-mail addresses: antoine_riaud@fudan.edu.cn (A. Riaud), jia.zhou@fudan.edu.cn (J. Zhou).
[1] These authors contribute equally to the work.

https://doi.org/10.1016/j.snb.2020.128763
Received 26 May 2020; Received in revised form 16 July 2020; Accepted 13 August 2020
Available online 18 August 2020

integration and compatibility with EWOD electrode arrays still require delicate and laborious manufacturing processes.

In addition to these electronic strategies, the pin-count can be further reduced by considering some practical constraints in EWOD design. For instance, droplets tend to be driven unidirectionally along separate paths because back-and-forth motion or path overlap would increase cross-contamination hazards [19,22,23]. Fan et al. [24,25] used the asymmetric electrowetting effect under opposed polarities to move droplets. However, their design necessitates nonlinear insulating materials that can only be actuated by direct current signals [25–27]. This restricts the types of dielectric materials, causes localized charge trapping [14], and increases contact angle hysteresis [28,29] that hinders the droplet motion [30]. Moreover, the droplet diameter, electrode size, actuation voltage, and signal switching frequency must be delicately adjusted based on manufacturing parameters and application scenarios to avoid irregular motion.

In this paper, we propose a multiplexed asymmetric electrode design for unidirectional droplet motion. Heart-shape electrodes ensure that the droplet overlaps more with the front electrode than with the rear one. The directional net capillary force exerted on the droplet can drive it over long distances using only two alternately applied actuation signals. The device principle is purely geometrical and does not rely on the actuation signal frequency. Each segment of the interconnection circuit spans only two electrode-lengths, which simplifies the circuit routing and avoids the possible trace overlap in large-scale electrode arrays. By minimizing the pin number, this design provides a promising strategy for electrode arrangement in multifunctional, large-scale EWOD platforms.

2. Experimental

2.1. Electrode design and working principle

The Lippmann-Young equation [2,3] describes the dependence of the contact angle θ on the applied voltage V as

$$\cos\theta - \cos\theta_0 = \frac{C}{2\gamma_{LG}}V^2, \tag{1}$$

where θ_0 is the contact angle without applied voltages, C is the areal capacitance between the electrode and the liquid (i.e. the specific capacitance of dielectric layers separating the electrode from the liquid), and γ_{LG} is the interfacial tension between the liquid and the surrounding medium like air or oil.

Following Jones et al. [31,32], Kang [33], and Zeng and Korsmeyer [34], the capillary force per unit length acting perpendicularly to the three-phase contact line (CL) of the droplet is given by

$$f = \gamma_{LG}\cos\theta. \tag{2}$$

The integration of f over the droplet's CL yields the capillary force on the droplet [33]. For a droplet actuated as shown in Fig. 1, we conclude that the net capillary force along the moving direction is [30,33]

$$F_{EWOD} = \int_{TCL} f\ \vec{n}\cdot\vec{i}\ \mathrm{d}l = L_E\gamma_{LG}(\cos\theta - \cos\theta_0), \tag{3}$$

where $\mathrm{d}l$ is a unit element of the CL, $\vec{n}$ is the normal unit vector of $\mathrm{d}l$, $\vec{i}$ is the unit vector in the moving direction, and L_E is the difference of projected lengths of the CLs on the two adjacent active electrodes. This simple model allows a quantitative analysis of many engineering problems [3,30,35–40].

Here, we consider an asymmetric electrode as shown in Fig. 1a. The electrode is designed like a heart with a wedge extending backward and a notch at the front end. By breaking the symmetry of the actuation electrode along the desired moving direction, the projected CL on the active electrode at the front of the droplet is made longer than the one at the back, resulting in a non-vanishing electro-capillary force driving the droplet to the right of Fig. 1a.

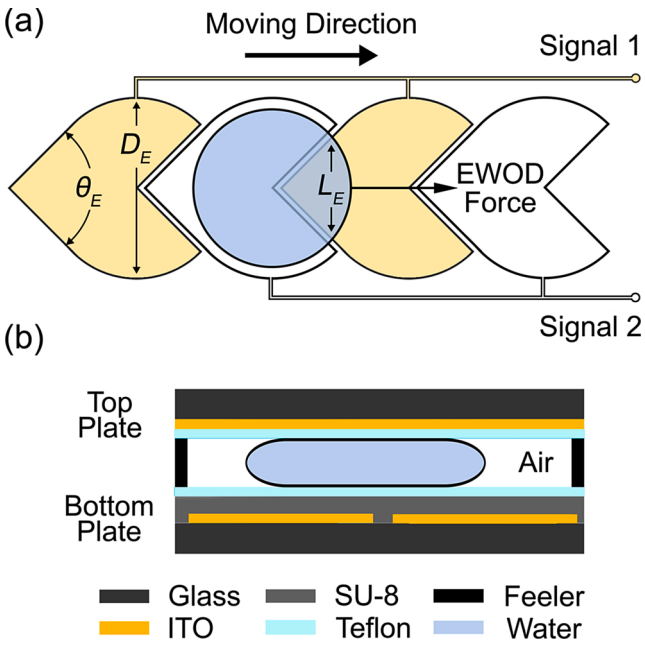

Fig. 1. Schematic of the EWOD device. (a) Asymmetric electrode design. Heart-shape electrodes are interconnected alternately to two power tracks of opposed activity. The diameter of the circular part is D_E and the angle of the wedge is θ_E. L_E refers to the vertical projection of the total CL on the active electrodes. The asymmetric shape of EWOD electrodes exerts a directional net capillary force on the droplet, resulting in a movement to the right. Electrodes are outlined with the active ones filled in yellow, and the droplet is outlined and filled in blue. (b) Side view of the two-plate EWOD structure.

Long-distance droplet transportation is achieved by forming a chain of asymmetric electrodes and alternately connecting them to two power tracks of opposed activity. Swapping the tracks activity (alternately ground and live wire) drives the droplet to move forward, as demonstrated below.

2.2. Fabrication of the EWOD device

We fabricated a two-plate EWOD device as sketched in Fig. 1b (See Fig. S1 in Supplementary Information for electrode arrangements in different experiments). In this proof-of-concept design, the angle of the wedge θ_E is 90° while the diameter of the circular part is denoted by D_E. The bottom plate electrodes were patterned on indium-tin-oxide (ITO) coated glass (purchased from Wesley Technology Co., Ltd) by standard photolithography and wet etching. The spacing between adjacent electrodes is 30 μm. SU-8 2002 (purchased from MicroChem) and Teflon® AF2400 (purchased from DuPont) were successively spin-coated on the surface as a dielectric layer (thickness of 1 μm) and a hydrophobic layer (thickness of 60 nm), respectively. The top plate was a uniform ITO glass spin-coated with a 60 nm-thick Teflon® AF2400 layer. The parallel plates were assembled with a homemade clamp and a feeler gauge was inserted to adjust the gap height.

2.3. Droplet volume

For most EWOD designs, the droplet size only admits a lower bound: the liquid can be stretched over several electrodes, but can only be moved reliably when the droplet meniscus overlaps with adjacent electrodes. However, our platform is more restrictive because electrodes in the array are interconnected alternately. Indeed, in order to ensure the directionalnet capillary force, the droplet should not overlap with the rear electrode, so its diameter cannot exceed D_E. Moreover, the droplet must overlap with the front electrode, therefore the droplet

footprint must exceed the inscribed circle of the electrode, which yields a diameter $D_E/2$. In our preliminary tests, we found that the droplet can be smoothly actuated only when the ratio of the droplet diameter to the electrode diameter D_E is between 0.8 and 1 due to the distortions from the ideal circular footprint. In this paper, the diameter of the droplet footprint area was maintained close to the electrode diameter D_E.

3. Results and discussion

3.1. Directional actuation of the droplet

To characterize the droplet actuation capability of the electrode array, experiments were carried out with deionized water and AC supply (1 kHz, 90 V_{rms}). The electrode diameter D_E is 1 mm and the gap height between parallel plates is 100 μm, corresponding to a droplet volume of 340 nL. Since both electrodes and droplets are transparent, we edited Fig. 2 and Fig. 3 to improve clarity: the electrodes are outlined with the active ones filled in yellow, and the droplet is outlined and filled in blue (unedited videos are available in Supplementary Information).

Fig. 2 is captured from the experimental observation (see Movie. S1 in Supplementary Information for the original video). With two

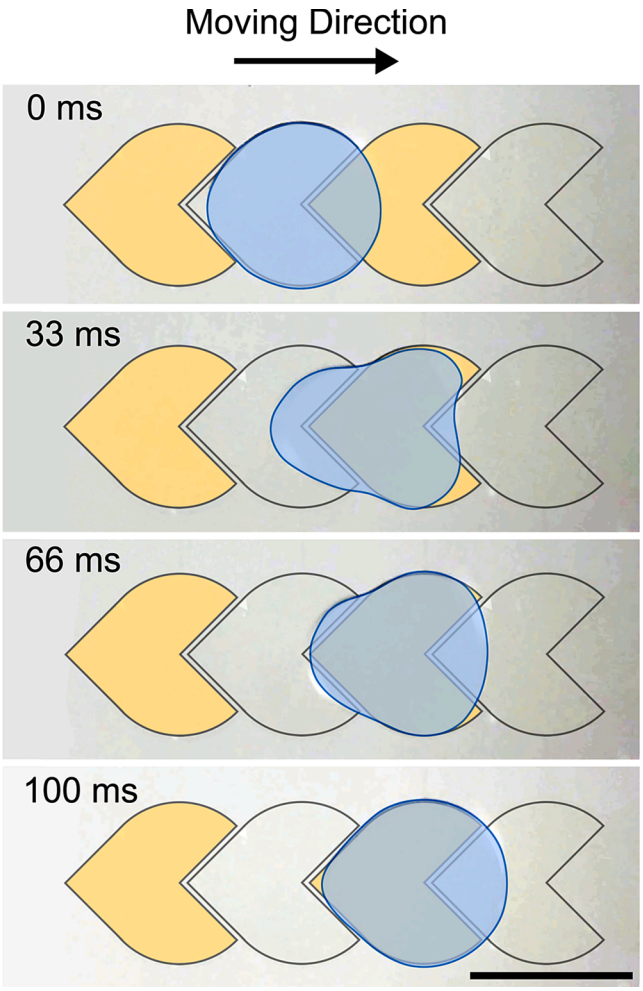

Fig. 2. Experimental observation of directional movement of one droplet. Experiments were carried out with AC supply (1 kHz, 90 V_{rms}). The electrode diameter is 1 mm and the gap height between parallel plates is 100 μm. The volume of the deionized water droplet is 340 nL. Since both electrodes and droplets are transparent, the figures were edited to improve clarity: electrodes are outlined with the active ones filled in yellow, and the droplet is outlined and filled in blue. See Movie. S1 in Supplementary Information for the original video. Scale bar: 1 mm.

electrodes adjacent to the droplet actuated (electrodes filled in yellow), the directional net capillary force drives the droplet to the active electrode on its right. The moving velocity is higher on both sides of the droplet but lower in the middle, consistent with the distribution of the projected CL on the active electrode. After the droplet has reached its final stable position, its footprint overlaps more with the front electrode than with the rear one. The liquid is therefore ready to move forward again.

Based on the working principle described above, synchronous transportation of multiple droplets can also be realized. The synchronous movement of two droplets is shown in Fig. 3 (captured from Movie. S2 in Supplementary Information). The movement starts when the front electrode is excited with the actuation voltage and terminates when the trailing edge of the droplet reaches the active electrode. After the droplets moved one electrode-length forward and reached a stable shape, the active states of the electrodes were swapped (see the color change of the electrode array in two columns of Fig. 3), which propels the droplets one electrode-length farther to the right. The alternating arrangement of active and passive electrodes ensures that there is at least one electrode between any two droplets, avoiding accidental coalescence.

Furthermore, by alternately actuating two sets of electrodes, the droplet requires only two actuation signals to travel across the entire electrode array. Fig. 4 shows such motion in a stacked micrograph captured from Movie. S3 in Supplementary Information with a 300 ms interval. The electrodes can be arranged in a straight line or polylines, allowing on-demand planning of the droplet (circuit) routing.

3.2. Actuation velocity of the asymmetric electrode

With the smartphone-based EWOD platform proposed previously [11,41], the droplets can be transported automatically at tunable signal switching speeds. The voltage-dependent maximum velocity at which droplets could be successfully transferred past 5 electrodes was recorded experimentally by changing the signal switching frequency. We also tested the influence of the electrode size (D_E = 1 mm, 1.5 mm, or 2 mm) and gap height (50 μm, 100 μm, or 150 μm, defined by the feeler gauge) on the droplet velocity. When changing these structural parameters, we ensured that the diameter of the droplet footprint area remained equal to the electrode diameter D_E.

Consistent with previous works [30,40,42], the maximum droplet velocity is approximately proportional to the square of the applied voltage in our experiments (see Fig. S2 in Supplementary Information for original data). Thus, we define the actuation capability as the fitted coefficient of the quadratic term. The actuation capability for different designs is shown in Fig. 5 (see Fig. S2 in Supplementary Information for original experimental data). Similar to our experimental measurements, Song et al. [30], Yafia and Najjaran [43], and Bahadur and Garimella [44] proposed predictions of the droplet motion velocity depending on the balance of the EWOD actuation force and the forces opposing droplet motion. For structures used in this work, the main opposing forces are: 1) the shear force due to the parallel plates, 2) the drag force exerted by the surrounding medium, and 3) the contact-line friction force. Based on their estimates, the maximum droplet moving velocity is approximately proportional to the gap height, but inversely proportional to the electrode diameter (and thus, the droplet diameter), consistent with our experimental observations.

Additionally, a threshold voltage V_{th} of about 50 V_{rms} is required to initiate droplet movement by overcoming the contact angle hysteresis (see Fig. S2 in Supplementary Information for original experimental data). Assuming that the contact angle hysteresis 2α is symmetric around the Lippmann-Young contact angle [39], Song et al. [30] evaluated the force balance on the droplet in a two-plate EWOD device and proposed the threshold voltage V_{th}:

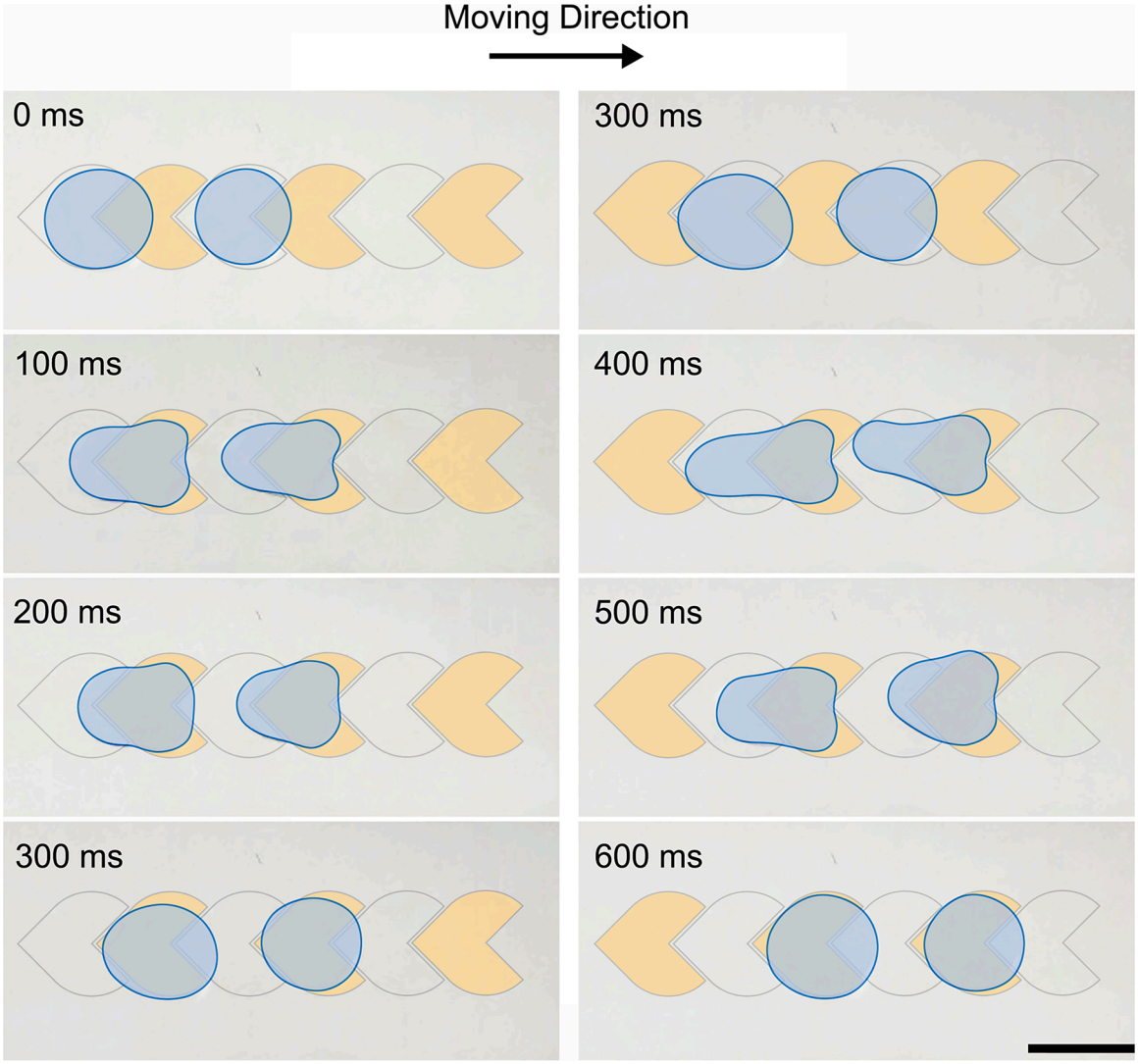

Fig. 3. Experimental observation of the synchronous directional movement of two droplets. See Movie. S2 in Supplementary Information for the original video. Scale bar: 1 mm.

Fig. 4. Experimental observation of long-distance directional droplet motions. The stacked photo demonstrates the droplet movement with a 300 ms interval. See Movie. S3 in Supplementary Information for the original video. Scale bar: 1 mm.

$$V_{th} = \sqrt{\frac{4\gamma_{LG}\sin\theta_0\tan\alpha - 4\gamma_{LG}\cos\theta_0\tan^2\alpha}{C + C\tan^2\alpha}} \quad (4)$$

In our experiments, the thicknesses of SU-8 2002 and Teflon® AF2400 layers are 1 μm and 60 nm, respectively. The equilibrium contact angle with no actuation voltage applied (θ_0) is 121° and the experimentally measured contact angle hysteresis 2α is about 8° (see Fig. S3 in Supplementary Information). The calculation with parameters used in our experiments gives $V_{th} \approx 32$ V, slightly lower than the experimental value (about 50 V_{rms}). V_{th} may be underestimated due to (i) the different electrode geometry and (ii) the distorted shape of the moving droplet. For the droplet actuated by heart-shape electrodes, the movement starts at the droplet meniscus in contact with the front active electrode, which then pulls the rest of the droplet forward. This process differs from the theoretical model where the motion is supposed to be simultaneous [30].

4. Conclusion

Pin-count minimization has emerged as a great challenge for large-scale digital microfluidic platforms. Taking advantage of the directional movement needed for most digital microfluidic systems to minimize cross-contamination, we propose an asymmetric electrode design for the directional movement of droplets with only two alternately applied actuation signals. With electrodes in the array interconnected alternately, each segment of the interconnection circuit spans only two electrode-lengths, greatly simplifying the circuit routing and avoiding the possible trace overlap. This design provides a simple approach for large-scale EWOD platforms with minimized pin number, especially for directional droplet transportation among functional zones for successive operations.

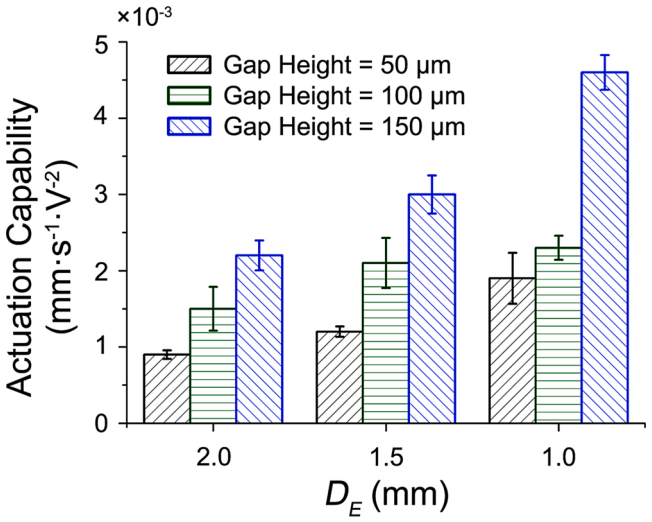

Fig. 5. Actuation capability of the asymmetric electrode. The velocity was calculated by experimentally measuring the time it takes the droplet to move past 5 electrodes. The maximum droplet velocity was found proportional to the square of the applied voltage in our experiments and the fitted coefficient of the quadratic term was defined as the actuation capability. The actuation capability in this figure was averaged over ten measurements with error bars the standard deviations. See Fig. S2 in Supplementary Information for original data.

CRediT authorship contribution statement

Wei Wang: Methodology, Investigation, Data curation, Writing - original draft. **Xichuan Rui:** Investigation, Data curation. **Wenjie Sheng:** Conceptualization, Methodology. **Qing Wang:** Writing - review & editing. **Qi Wang:** Writing - review & editing. **Kaidi Zhang:** Methodology, Resources. **Antoine Riaud:** Supervision, Writing - review & editing. **Jia Zhou:** Supervision, Resources, Writing - review & editing, Project administration.

Declaration of Competing Interest

There are no conflicts of interest to declare.

Acknowledgements

This work was supported by the National Natural Science Foundation of China with Grant No. 61874033 and No. 61674043, the Natural Science Foundation of Shanghai Municipal Government with Grant No. 18ZR1402600, and the State Key Laboratory of ASIC and System, Fudan University with Grant No. 2018MS003.

Appendix A. Supplementary data

Supplementary material related to this article can be found, in the online version, at doi:https://doi.org/10.1016/j.snb.2020.128763.

References

[1] R.B. Fair, Digital microfluidics: is a true lab-on-a-chip possible? Microfluid. Nanofluid. 3 (2007) 245–281, https://doi.org/10.1007/s10404-007-0161-8.
[2] F. Mugele, J.C. Baret, Electrowetting: From basics to applications, J. Phys. Condens. Matter 17 (2005) R705–R774, https://doi.org/10.1088/0953-8984/17/28/r01.
[3] S.K. Cho, H.J. Moon, C.J. Kim, Creating, transporting, cutting, and merging liquid droplets by electrowetting-based actuation for digital microfluidic circuits, J. Microelectromech. Syst. 12 (2003) 70–80, https://doi.org/10.1109/jmems.2002.807467.
[4] X. Min, W.S. Kim, Beyond high voltage in the digital microfluidic devices for an integrated portable sensing system, Microfluid. Nanofluid. 23 (2019) 14, https://doi.org/10.1007/s10404-019-2294-y.
[5] P.C. Teng, D.L. Tian, H.Y. Fu, S.T. Wang, Recent progress of electrowetting for droplet manipulation: from wetting to superwetting systems, Mat. Chem. Front. 4 (2020) 140–154, https://doi.org/10.1039/c9qm00458k.
[6] L. Malic, D. Brassard, T. Veres, M. Tabrizian, Integration and detection of biochemical assays in digital microfluidic LOC devices, Lab Chip 10 (2010) 418–431, https://doi.org/10.1039/b917668c.
[7] S.K. Fan, F.M. Wang, Multiphase optofluidics on an electro-microfluidic platform powered by electrowetting and dielectrophoresis, Lab Chip 14 (2014) 2728–2738, https://doi.org/10.1039/c4lc00317a.
[8] B. Hadwen, G.R. Broder, D. Morganti, A. Jacobs, C. Brown, J.R. Hector, et al., Programmable large area digital microfluidic array with integrated droplet sensing for bioassays, Lab Chip 12 (2012) 3305–3313, https://doi.org/10.1039/c2lc40273d.
[9] S. Kalsi, M. Valiadi, M.-N. Tsaloglou, L. Parry-Jones, A. Jacobs, B. Watson, et al., Rapid and sensitive detection of antibiotic resistance on a programmable digital microfluidic platform, Lab Chip 15 (2015) 3065–3075, https://doi.org/10.1039/c5lc00462d.
[10] J.H. Noh, J. Noh, E. Kreit, J. Heikenfeld, P.D. Rack, Toward active-matrix lab-on-a-chip: programmable electrofluidic control enabled by arrayed oxide thin film transistors, Lab Chip 12 (2012) 353–360, https://doi.org/10.1039/c1lc20851a.
[11] C. Li, K. Zhang, X. Wang, J. Zhang, H. Liu, J. Zhou, Feedback control system for large scale 2D digital microfluidic platforms, Sens. Actuators B Chem. 255 (2018) 3616–3622, https://doi.org/10.1016/j.snb.2017.09.071.
[12] G. Jian, C.J. Kim, Direct-referencing two-dimensional-array digital microfluidics using multilayer printed circuit board, J. Microelectromech. Syst. 17 (2008) 257–264, https://doi.org/10.1109/JMEMS.2007.912698.
[13] D. Grissom, C. Curtis, S. Windh, C. Phung, N. Kumar, Z. Zimmerman, et al., An open-source compiler and PCB synthesis tool for digital microfluidic biochips, Integration 51 (2015) 169–193, https://doi.org/10.1016/j.vlsi.2015.01.004.
[14] H. Wu, R. Dey, I. Siretanu, D. van den Ende, L. Shui, G. Zhou, et al., Electrically controlled localized charge trapping at amorphous fluoropolymer-electrolyte interfaces, Small 16 (2020) 1905726, https://doi.org/10.1002/smll.201905726.
[15] S.-H. Yeh, J.-W. Chang, T.-W. Ho, S.-T. Yu, T.-Y. Ho, Voltage-aware chip-level design for reliability-driven pin-constrained EWOD chips, IEEE T. Comput. Aid D. 33 (2014) 1302–1315, https://doi.org/10.1109/TCAD.2014.2331340.
[16] P. Roy, S. Saha, H. Rahaman, P. Dasgupta, Novel wire planning schemes for pin minimization in digital microfluidic biochips, IEEE T. VLSI Syst. 24 (2016) 3345–3358, https://doi.org/10.1109/TVLSI.2016.2541671.
[17] S.K. Fan, C. Hashi, C.J. Kim, Manipulation of multiple droplets on N×M grid by cross-reference EWOD driving scheme and pressure-contact packaging, in: IEEE the Sixteenth International Conference on Micro Electro Mechanical Systems, Kyoto, Japan, 23-23 Jan, 2003, https://doi.org/10.1109/MEMSYS.2003.1189844.
[18] Y. Zhao, T. Xu, K. Chakrabarty, Broadcast electrode-addressing and scheduling methods for pin-constrained digital microfluidic biochips, IEEE T. Comput. Aid D. 30 (2011) 986–999, https://doi.org/10.1109/tcad.2011.2116250.
[19] T.W. Huang, S.Y. Yeh, T.Y. Ho, A network-flow based pin-count aware routing algorithm for broadcast-addressing EWOD chips, in: 2010 IEEE/ACM International Conference on Computer-Aided Design (ICCAD), San Jose, CA, USA, 7-11 Nov, 2010, https://doi.org/10.1109/ICCAD.2010.5653715.
[20] T.A. Dinh, S. Yamashita, T.Y. Ho, An optimal pin-count design with logic optimization for digital microfluidic biochips, IEEE T. Comput. Aid D. 34 (2015) 629–641, https://doi.org/10.1109/tcad.2015.2394502.
[21] D.T. Grissom, J. McDaniel, P. Brisk, A low-cost field-programmable pin-constrained digital microfluidic biochip, IEEE T. Comput. Aid D. 33 (2014) 1657–1670, https://doi.org/10.1109/TCAD.2014.2347931.
[22] S.Y. Liu, C.H. Chang, H.M. Chen, T.Y. Ho, ACER: An agglomerative clustering based electrode addressing and routing algorithm for pin-constrained EWOD chips, IEEE T. Comput. Aid D. 33 (2014) 1316–1327, https://doi.org/10.1109/tcad.2014.2329415.
[23] C. Li, W. Wei, C. Lei, X. Ji, Z. Jia, Detection of faults and barriers on automated large-scale 2-D EWOD digital microfluidics, J. Microelectromech. Syst. 26 (2017) 1449–1456, https://doi.org/10.1109/JMEMS.2017.2764139.
[24] T.-T. Wang, P.-W. Huang, S.-K. Fan, Droplets oscillation and continuous pumping by asymmetric electrowetting, in: 19th IEEE International Conference on Micro Electro Mechanical Systems, Istanbul, Turkey, 22-26 Jan, 2006, https://doi.org/10.1109/MEMSYS.2006.1627764.
[25] S.K. Fan, H. Yang, T.-T. Wang, W. Hsu, Asymmetric electrowetting—moving droplets by a square wave, Lab Chip 7 (2007) 1330–1335, https://doi.org/10.1039/b704084a.
[26] E. Seyrat, R.A. Hayes, Amorphous fluoropolymers as insulators for reversible low-voltage electrowetting, J. Appl. Phys. 90 (2001) 1383, https://doi.org/10.1063/1.1383583.
[27] M.W.J. Prins, Reversible electrowetting and trapping of charge : model and experiments, Langmuir 15 (1999) 6616–6620, https://doi.org/10.1021/la990548n.
[28] F. Li, F. Mugele, How to make sticky surfaces slippery: Contact angle hysteresis in electrowetting with alternating voltage, Appl. Phys. Lett. 92 (2008) 244108, https://doi.org/10.1063/1.2945803.
[29] W.C. Nelson, P. Sen, C.-J. Kim, Dynamic contact angles and hysteresis under electrowetting-on-dielectric, Langmuir 27 (2011) 10319–10326, https://doi.org/10.1021/la2018083.
[30] J.H. Song, R. Evans, Y.Y. Lin, B.N. Hsu, R.B. Fair, A scaling model for electrowetting-on-dielectric microfluidic actuators, Microfluid. Nanofluid. 7 (2009) 75–89, https://doi.org/10.1007/s10404-008-0360-y.

[31] T.B. Jones, J.D. Fowler, Y.S. Chang, C.J. Kim, Frequency-based relationship of electrowetting and dielectrophoretic liquid microactuation, Langmuir 19 (2003) 7646–7651, https://doi.org/10.1021/la0347511.
[32] T.B. Jones, An electromechanical interpretation of electrowetting, J. Micromech. Microeng. 15 (2005) 1184–1187, https://doi.org/10.1088/0960-1317/15/6/008.
[33] H.K. Kang, How electrostatic fields change contact angle in electrowetting, Langmuir 18 (2002) 10318–10322, https://doi.org/10.1021/la0263615.
[34] J. Zeng, T. Korsmeyer, Principles of droplet electrohydrodynamics for lab-on-a-chip, Lab Chip 4 (2004) 265–277, https://doi.org/10.1039/B403082F.
[35] I. Moon, J. Kim, Using EWOD (electrowetting-on-dielectric) actuation in a micro conveyor system, Sens. Actuators A Phys. 130-131 (2006) 537–544, https://doi.org/10.1016/j.sna.2005.12.016.
[36] J. Berthier, P. Clementz, O. Raccurt, D. Jary, P. Claustre, C. Peponnet, et al., Computer aided design of an EWOD microdevice, Sens. Actuators A Phys. 127 (2006) 283–294, https://doi.org/10.1016/j.sna.2005.09.026.
[37] L.Y. Yeo, H.C. Chang, Electrowetting films on parallel line electrodes, Phys. Rev. E 73 (2006) 011605, https://doi.org/10.1103/physreve.73.011605.
[38] L.Y. Yeo, H.-C. Chang, Static and spontaneous electrowetting, Mod. Phys. Lett. B 19 (2005) 549–569, https://doi.org/10.1142/s0217984905008542.
[39] J. Berthier, P. Dubois, P. Clementz, P. Claustre, C. Peponnet, Y. Fouillet, Actuation potentials and capillary forces in electrowetting based microsysterns, Sens. Actuators A Phys. 134 (2007) 471–479, https://doi.org/10.1016/j.sna.2006.04.050.
[40] J. Chen, Y. Yu, J. Li, Y. Lai, J. Zhou, Size-variable droplet actuation by interdigitated electrowetting electrode, Appl. Phys. Lett. 101 (2012) 234102, https://doi.org/10.1063/1.4769433.
[41] Z. Zhi, K. Zhang, W. Wei, W. Xu, Z. Jia, Portable electrowetting digital microfluidics analysis platform for chemiluminescence sensing, IEEE Sens. J. 16 (2016) 4531–4536, https://doi.org/10.1109/JSEN.2016.2544356.
[42] J. Chen, Y. Yu, K. Zhang, C. Wu, Q.L. Ai, Z. Jia, Study of cyanoethyl pullulan as insulator for electrowetting, Sens. Actuators B Chem. 199 (2014) 183–189, https://doi.org/10.1016/j.snb.2014.03.112.
[43] M. Yafia, H. Najjaran, High precision control of gap height for enhancing principal digital microfluidics operations, Sens. Actuators B Chem. 186 (2013) 343–352, https://doi.org/10.1016/j.snb.2013.06.029.
[44] V. Bahadur, S.V. Garimella, An energy-based model for electrowetting-induced droplet actuation, J. Micromech. Microeng. 16 (2006) 1494–1503, https://doi.org/10.1088/0960-1317/16/8/009.

Wei Wang is currently pursuing a doctoral degree in the State Key Laboratory of ASIC and System, School of Microelectronics, Fudan University. His research focuses on biological and chemical applications of microfluidic technologies.

Xichuan Rui is currently pursuing a doctoral degree in the State Key Laboratory of ASIC and System, School of Microelectronics, Fudan University. His research focuses on digital microfluidic devices and their applications in PCR.

Wenjie Sheng received her master's degree from the State Key Laboratory of ASIC and System, School of Microelectronics, Fudan University. Her research focuses on biological and chemical applications of microfluidic technologies.

Qing Wang is currently pursuing a doctoral degree in the State Key Laboratory of ASIC and System, School of Microelectronics, Fudan University. Her research focuses on photo-acoustic tweezers in microfluidic systems.

Qi Wang is currently pursuing her master's degree from the State Key Laboratory of ASIC and System, School of Microelectronics, Fudan University. Her research focuses on the particle screening and device reliability in microfluidic systems.

Kaidi Zhang is currently pursuing a doctoral degree in the State Key Laboratory of ASIC and System, School of Microelectronics, Fudan University. His research interest focuses on digital microfluidic devices and their applications in biology.

Antoine Riaud received his Master degree in Chemical Engineering at Tsinghua University and his Ph.D. in physical acoustics and microelectronics at Pierre and Marie Curie University and Lille University. He is currently an Associate Professor in the State Key Laboratory of ASIC and System, School of Microelectronics, Fudan University. His research interests are in acoustic streaming in microdroplets, acoustic tweezers, and multiphase microflow modeling.

Jia Zhou received the Ph.D. degree from Fudan University in 2004. She is currently a Professor in the State Key Laboratory of ASIC and System, School of Microelectronics, Fudan University. Her research interests are in nano/microfluidics, MEMS/NEMS-based chemical, biochemical and biomedical sensors.